

Dissipation and dynamics in ultrafast intersystem crossings

Michel van Veenendaal^{1,2}¹*Department of Physics, Northern Illinois University, DeKalb, Illinois 60115, USA*²*Advanced Photon Source, Argonne National Laboratory, 9700 South Cass Avenue, Argonne, Illinois 60439, USA^a*

(Dated: 14 June 2020)

The effects of dynamics and dissipation on ultrafast intersystem crossings is studied for a dissipative two-level system coupled to a local vibronic mode. A method of amplitude damping of the wave packet is presented that account better for the position of the wave packet and avoids spurious transitions between potential wells. It is demonstrated that Fermi's golden rule, the typical semiquantitative approach to extract population transfer rates from potential landscapes, only holds under limited conditions. Generally, the effects of dynamics and dissipation lead to deviations from the expected exponential population transfer, strong changes in transfer times and total population transfer, and significant recurrence or "spillover" of the wave packet.

PACS numbers: 34.30.+h,03.65.Yz,82.50.Hp

Keywords: Intersystem crossings, nonequilibrium dynamics

I. INTRODUCTION

Intersystem crossings are nonradiative transitions between different electronic states and play an important role in many important phenomena, such as ultrafast phase transitions, catalysis, and photosynthesis. A prototypical example is the spin crossover where after photoexcitation the total spin on an ion changes^{1,2}. These transitions can occur on a femtosecond timescale and have been intensively studied using pump-probe experiments in the optical and X-ray range³⁻⁸. Although these transitions often occur in large organometallic complexes, the important intersystem crossings often occur on the metal ion. The role of the ligands surrounding the ion is to provide the vibronic modes responsible for the intersystem crossings and dissipate energy away from the metal ion. Due to the complexity of the problem, the theoretical study of these effects generally involves approximations (for a recent review, see Ref.⁹). There are several essential ingredients in the description of intersystem crossings. First, a coupling between the different electronic states is needed. This is not necessarily a large interaction, but can require certain characteristics. For example, for spin crossovers, the spin-orbit interaction allows the coupling between states with different total spins. Secondly, the electronic states generally require a different coupling to the local vibronic states. This leads to the creation of a wave packet allowing the system to nonadiabatically "move away" from the initial state or, in more quantum mechanical terms, it provides a continuum that causes a dephasing into the new state¹⁰. In the absence of such a vibronic coupling to the nuclear degrees of freedom, the system simply oscillates between the two electronic states. Additional approximations then allow the determination of exponential decay rates between the

different electronic states in terms of the electronic and vibronic coupling constants.

In this paper, the focus is on intersystem crossings such as those occurring on metallic sites in large organometallic systems. An estimate of the population transfer between different states can be obtained from Fermi's golden rule, which predicts an exponential decay between the states proportional to the coupling constant. However, this paper demonstrates that, even for simple systems, additional phenomena can drastically affect the time-dependence and the total population transfer between the states. First, energy redistribution: in order to obtain a qualitative understanding of the intersystem crossing, one would like to define a small system containing the electronic states and the most relevant local vibronic modes, typically stretching modes, such as breathing modes and Jahn-Teller distortions. These are generally sufficient to create a wave packet that moves away from the initial state. However, when the system is small and energy is conserved, a recurrence to the initial state occurs typically after an oscillation period of the relevant vibronic modes. There are two different ways to prevent this. One can take a larger system allowing the energy to be distributed over additional modes, such as bending modes or more delocalized vibrations. This is, for example, achieved by treating the nuclear motion classically resulting in a time-dependent potential landscape in which the electronic wave packet propagates¹¹⁻²¹. While these calculations are very important, they strongly increase the size of the calculation. Additionally, the larger system generally forces the choice of a particular compound making it difficult to study trends. The other option, the approach taken in this paper, is to keep the system small and remove energy via damping/dissipation. However, this requires the inclusion of dissipation in quantum mechanics which complicates the calculation²²⁻²⁴.

The second important aspect is dynamics. In calculating intersystem crossing rates, using, for example,

^aElectronic mail: veenendaal@niu.edu

Fermi's golden rule, the nature of the wave packet only enters in the Franck-Condon factors that determine the intersystem crossing rates⁹. The time dependence is given by the exponential decay resulting from the dephasing of the initial state into the continuum of vibronic states. A dynamical calculation on a larger system can often provide detailed information on the wave packet propagation and the nuclear displacement. However, the restriction to a particular system again complicates our understanding what aspects of the dynamics are really crucial for the intersystem crossing.

In this paper, the role of dynamics and dissipation in the intersystem crossing rates are discussed. The model is a two-level system coupled to a local vibronic mode. The treatment is fully quantum-mechanical and includes quantum-mechanical dissipation of the wave packet. It is demonstrated that approximations, such as Fermi's golden that only consider the static electronic and vibronic structure, can only explain the intersystem crossings in certain limiting cases. In general, a more complex picture emerges where dissipation and dynamics can significantly change the population transfers.

II. MODEL AND BACKGROUND

One of the simplest models to describe intersystem crossings for a localized electronic system coupled to a vibronic mode is given by the following Hamiltonian

$$H = \sum_i [E_i - \lambda_i(a + a^\dagger)] c_i^\dagger c_i + V(c_2^\dagger c_1 + \text{H.c.}) + \hbar\omega_0 a^\dagger a, \quad (1)$$

which describes two levels with energy E_i indexed by $i = 1, 2$; c_i^\dagger creates an electron in state i and a^\dagger and a are raising and lowering operators for the local vibronic mode. The electronic states are coupled to each with a strength V . The levels couple differently to a local vibronic mode where ω_0 is the angular frequency of the vibronic mode. A value of $\hbar\omega_0 = 30$ meV is taken. Typical values for the parameters are taken throughout the paper to obtain a better feeling of the timescales. This mode is typically a stretching mode such as a breathing mode or a Jahn-Teller distortion, which couple more strongly to the electronic structure than bending modes. The coupling between the electronic and vibronic states is given by the second term on the right-hand side and has a coupling strength λ_i for state i . λ_i can be positive or negative reflecting a displacement in the positive or negative direction, respectively. For uncoupled states ($V = 0$), the coupling to the vibrational mode leads to eigenstates $|n_i\rangle$ with eigenenergies $E_{n_i} = E_i - \varepsilon_i + n_i\hbar\omega$, where the polaronic coupling is given by $\varepsilon_i = \lambda_i^2/\hbar\omega_0$. The expectation value of the renormalized position operator $\bar{x} = \sqrt{m\omega_0/\hbar}x = (a + a^\dagger)/\sqrt{2}$ is $\langle n_i|\bar{x}|n_i\rangle = \sqrt{2}\lambda_i/\hbar\omega_0$.

The typical understanding of the decay constant for intersystem crossings starts out with the system initially

in one of the states, say $|n_1\rangle$ with energy $E_{n_1} = E_1 + n_1\hbar\omega_0$ (we set $\varepsilon_1 \equiv 0$, which can be done without any loss of generality). This state couples via V to the vibronic states $|n_2\rangle$ with energy $E_{n_2} = E_2 - \varepsilon_2 + n_2\hbar\omega_0$. To lowest order, the Green's function for this problem is given by

$$G_{n_1}(\omega) \cong \frac{1}{\hbar\omega - E_{n_1} - \sum_{n_2} \frac{V^2 |\langle n_2|c_2^\dagger c_1|n_1\rangle|^2}{\hbar\omega + E_{n_1} - E_{n_2}}}. \quad (2)$$

Due to the vibronic coupling the matrix elements between the different states have a factor $\langle n_2|c_2^\dagger c_1|n_1\rangle$ which are the Franck-Condon factors. The Green's function is comparable to that of the well-known Fano problem¹⁰ of a state coupled to a continuum. Due to the dephasing into the continuum, the occupation of state 1 exponentially decreases as $n_1(t) = e^{-k_0 t}$. The decay constant k_0 , with

$$k_0 = \frac{2\pi}{\hbar} V^2 \sum_{n_2} |\langle n_2|c_2^\dagger c_1|n_1\rangle|^2 \delta(E_{n_2} - E_{n_1}), \quad (3)$$

is essentially given by Fermi's golden rule describing all the possible transitions between state 1 and 2

This result is nice and often used since it gives an exponential rate of population transfer expressed in terms of the coupling constant and Franck-Condon factors. It often gives a very good idea of the decay for an "optimal" intersystem crossing, where optimal means the situation where the potential energy curve of state 2 crosses the minimum of that of state 1, see the inset of Fig. 1, and the initial state is $|n_1 = 0\rangle$. The dashed line in Fig. 1 shows the occupation of state $n_1(t)$ as a function of time following Fermi's golden rule. This should be compared to the exact solution of Eq. (1) given by the red line. Up to $t \cong 80$ fs, there is a very good agreement with the exponential decay. The decay constant k is calculated by replacing the discrete vibronic states with a density of states representing the Franck-Condon coupling, $\rho(\omega) = e^{-g} g^{\omega/\omega_0} / [\hbar\omega_0 \Gamma(\omega/\omega_0 + 1)]$ with $g = \varepsilon_2/\hbar\omega_0$ and $\Gamma(x)$ is the gamma function. This gives $k_0 = 2\pi V^2 \rho(\varepsilon_2 + E_1 - E_2)/\hbar$ in units of s^{-1} . The actual value used is $k = \kappa k_0$. The factor $\kappa \cong 0.5-1$ corrects for additional effects to be discussed below with $\kappa \rightarrow 1$ for $V \rightarrow 0$. The value used here is $\kappa = 0.72$.

However, at some point the occupation of state 1 from the exact solution starts to increase again. The underlying reason is easily understood: the wave packet travels through the second potential well and after one period $T_0 = 2\pi/\omega_0 = 138$ fs the wave packet is back at its starting position. Or, in other words, since the initial state does not couple to a real continuum but to a set of vibronic states, a recurrence of the initial state is observed. There are different ways to increase the recurrence time or suppress the recurrence. First, the system size can be increased by coupling the local vibronic mode to other local modes (for example, bending modes) or by letting the vibrational energy spread out over a larger system¹¹⁻²¹. However, since this paper is more concerned with trends

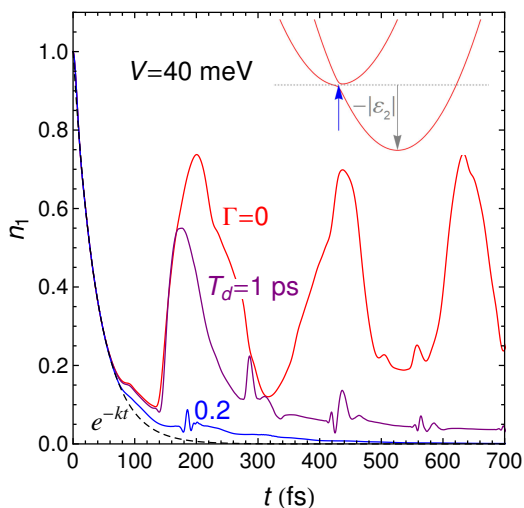


FIG. 1. Time dependence of the occupation $n_1(t)$ of state 1 as a function of different decay times $T_d = 1/\Gamma$ of the dissipation of the vibronic mode (values indicated in the Figure). Other parameters are $E_2 - E_1 = 0$, $\varepsilon_2 = 1$ eV, $\hbar\omega_0 = 30$ meV, and $V = 40$ meV. The inset shows the semiclassical potential energy curve. The blue arrow indicates the initial position.

as a function of coupling constants, displacements, and dissipation, energy is removed from the system via quantum dissipation^{22–25}.

Here, dissipation is included via amplitude damping of the vibronic mode. The method is closely related to that of Ref.^{25–27}. The wave packet $|\psi(t)\rangle = \sum_m c_m(t)|m\rangle$ is described in terms of all the states $|m\rangle$ of the system. The wave packet couples linearly to the surroundings and the probability of losing a vibrational quantum $\hbar\omega_0$ is proportional to the number of excited vibronic states, *i.e.* $n|\psi(t)\rangle = \sum_m \alpha_m(t)|m\rangle$, where $n = a^\dagger a$ is the number operator. The state that is reached after losing $\hbar\omega_0$ is $a|\psi(t)\rangle = \sum_m \beta_m(t)|m\rangle$. For amplitude damping, this affects the probabilities $P_m(t) = |c_m(t)|^2$ of the wave packet. The change in the probabilities at a particular time is given by

$$\frac{dP_m(t)}{dt} = 2\Gamma(-c_m^*(t)\alpha_m(t) + |\beta_m(t)|^2), \quad (4)$$

where the damping constant Γ reflects the amount of coupling of the local system to the surroundings. For a single potential well, this mechanism causes a simple exponential damping. Taking $\varepsilon = 0$, a wave packet can be created by taking the eigenstate for a finite ε_0 (a displaced harmonic oscillator state) as the initial state. The renormalized initial amplitude of the oscillation is given by $\bar{x}(0) = \sqrt{2}\lambda_i/\hbar\omega_0$. In the presence of damping, the time dependence of the renormalized amplitude is given by $\bar{x}(t) = \bar{x}^0 e^{-\Gamma t} \cos\omega_0 t$. The energy damps as $E(t) = \varepsilon_0 e^{-2\Gamma t}$ with $\varepsilon_0 = \lambda_0^2/\hbar\omega_0$.

The advantage of this approach of damping the wave packet over earlier work^{25–27} is a better treatment of the position of the wave packet. The correction is important for damping involving strongly coupled eigenstates.

This can be most easily seen by considering the limit $\hbar\omega_0 \gg V$ when eigenstates can be viewed as combinations of states in different potential wells that are closest in energy, such as $|E_{nn'}^+\rangle = \cos\theta|1;n\rangle + \sin\theta|2;n'\rangle$ and $|E_{nn'}^-\rangle = \sin\theta|1;n\rangle - \cos\theta|2;n'\rangle$. Now let us consider a wavefunction $|\psi\rangle$ containing both eigenstates. For a dissipation mechanism based on eigenfunctions, applying the lowering operator on the eigenstates $a|E_{nn'}^\pm\rangle$ would allow for decay in both states 1 and 2. However, this is not always physically realistic since, for example, the wavefunction $|\psi\rangle = \cos\theta|E_{nn'}^+\rangle + \sin\theta|E_{nn'}^-\rangle = |1;n\rangle$ only contains state 1 and therefore the lowering operator a should not cause a transition to state 2. Note that eigenstates can be combinations of states 1 and 2 even in the case $V = 0$, simply due to accidental degeneracies. A dissipation mechanism based on eigenstates in the wavefunction could then give completely spurious transitions between state 1 and 2. It is therefore preferable to use a dissipation mechanism that works directly on the wavefunction.

The results for different decay times $T_d = 1/\Gamma$ are shown in Fig. 1. For $T_d = 1$ ps, the first recurrence starting around $T_0 = 138$ fs is still strong. However, subsequent recurrences at $t \cong nT_0$ with $n = 2, 3, \dots$ are suppressed. The underlying physics is clear: by extracting kinetic energy out of the oscillation, the wave packet can no longer reach the displacement x where the potential energy curves cross, see the inset of Fig. 1. A further decrease of the decay time leads to a further suppression of the recurrences. For $T_d = 0.2$ ps, there is a satisfactory agreement with the simple exponential decay e^{-kt} .

Whereas this seems to vindicate the Fermi golden rule approach, there are some definite limitations to this approach, not only numerically, but also from a conceptual point of view. Expressing the rate of population transfer k as a single constant omits most aspects of the dynamics of the wave packet and assumes that the dynamics can be simply described in terms of an exponential decay. Additionally, k is independent of the dissipation or the delocalization of the kinetic energy in the wave packet. It will be demonstrated that dynamics and dissipation can significantly change this picture of a simple exponential decay with a rate transfer expressed in terms of coupling constants.

III. RESULTS

A. Breakdown of Fermi's golden rule

In the previous Section, we saw that Fermi's golden rule gives a satisfactory description as long as the recurrences are sufficiently suppressed, either by including the delocalization or, as is done here, the damping of the oscillatory motion of the vibronic state. For the choice of parameters, this works well for a damping time of $T_d = 0.2$ ps. Let us first look at the limitations of Fermi's golden rule. For $V = 20$ meV (red), the numerical results are close to the $n_1(t) = e^{-k_0 t}$ dependence, where k_0 is

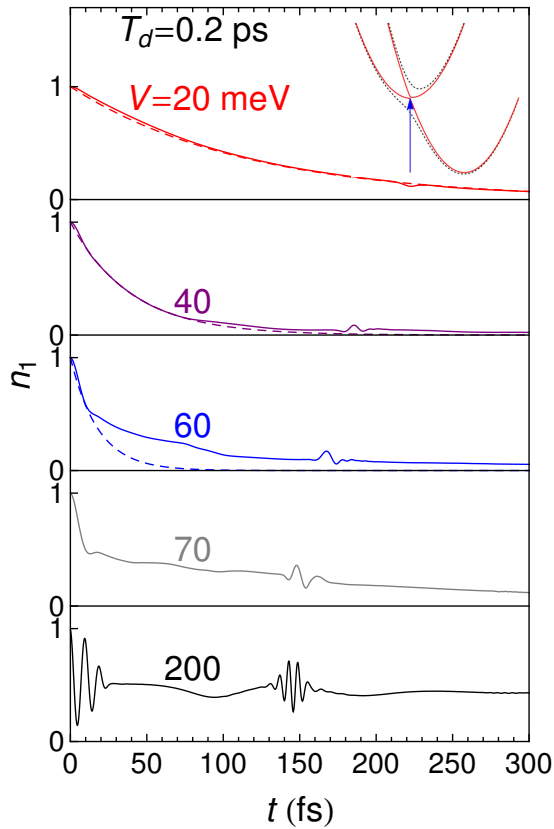


FIG. 2. Dependence of the occupation $n_1(t)$ on the coupling constant V for a fixed damping time $T_d = 0.2$ ps. The values of V go from 20 (red) to 200 (black) meV and are indicated in the Figure. The inset shows the potential energy for $V = 20$ (red) and 200 (black dotted) meV. The initial state is $|n_1 = 0\rangle$.

the rate of population transfer calculated using Fermi's golden rule, see Fig. 2. The recurrences are sufficiently suppressed. We already looked at $V = 40$ meV and noted that k_0 had to be scaled down to $k = \kappa k_0$ with $\kappa = 0.72$. Note that deviations from the exponential behavior occur around 80 fs. The V^2 dependence in Fermi's golden rule in Eq. (3) would lead one to expect that increasing V would lead to a faster decay. However, for $V = 60$ meV (blue line), the decay is initially faster, but then slows down and starts to deviate from the $n_1(t) = e^{-kt}$ (dashed blue line) and, around 50 fs, it becomes less efficient than the smaller coupling of $V = 40$ meV, see Fig. 2. The situation becomes even worse for $V = 70$ (gray) and 200 meV (black). Let us look at the latter to understand what is happening. For larger values of V , the decay problem effectively splits into two and can no longer be viewed as a state coupled to a continuum of vibronic states, but becomes two separate potential wells, see the inset in Fig. 2. For $V = 200$ meV, the part of the wave packet in the lower potential well decays very quickly with $1/k \cong 3.8$ fs and n_1 decreases to approximately 0.5. The remainder of the population in state 1 is predominantly associated with the potential well that is higher in energy. Initially,

there are strong oscillations. These occur because of the coupling between the two potential wells. The expected oscillation period for $V = 200$ meV is $h/(2V) \cong 10$ fs. A recurrence of these oscillations occurs around $T_0 \cong 138$ fs when the part of the wave packet in the lower potential well returns to the crossing of the two potential curves. Further recurrences are suppressed by the damping of the oscillatory motion. Upon closer inspection, we observe two decay times: an initial fast decay increasing with V due to the dephasing of the initial state into the vibronic levels of the other state followed by a slow decay decreasing with V . The second decay is actually due to the damping mechanism, which causes a coupling between the two potential wells. The crossing from the higher into the lower potential well is followed by a fast relaxation in the lower well. The relaxation between the wells occurs because they are not harmonic and the lowering operator couples them. This coupling decreases for larger V , since the wells become more parabolic. Therefore, even for an optimal configuration of an intersystem crossing, the population transfer rate k is only valid for small V and at small times. For longer timescales, the dissipation mechanism becomes dominant term in determining the rate of transfer of the population from state 1 to 2.

B. Displaced transitions

In addition to limitations with respect to the coupling constant, the derivation of Fermi's rule does not include aspects of dynamics. To get an idea of the effects of dynamics, the initial state is no longer assumed to be the lowest state of the first potential ($|n_1 = 0\rangle$), but a state displaced from the equilibrium, see the inset of Fig. 3. To obtain these states, it is assumed that the initial state is due to a photoexcitation from the ground state of a displaced potential well. Figure 3 shows the results for different displacements indicated in the Figure.

There are several differences of the calculations compared to those expected from Fermi's golden rule. First, let us first consider the population transfer rates. For Fermi's golden rule, the change in population transfer rate k is due to the energy dependence of the Franck-Condon factors. For the optimal intersystem crossing configuration, the Franck-Condon factors are maximum for $x(0) = 0$, *i.e.* the minimum of the parabolic potential well for state 1. Moving away from the minimum (see the values in Fig. 3 and the vertical lines in the inset), the excitation energy increases and the smaller Franck-Condon factors in Eq. (3) should reduce the coupling between the states. For example, for states 0.4-0.5 eV above the minimum, the expected population transfer times are $1/k \cong 500-1800$ fs. Although there is a slowing down of the population transfer, even for the maximum displacement of $x(0)/x_2 = -0.63$ (0.5 eV above the minimum), where x_2 is the displacement between the minima of the potential wells, the time to reach e^{-1} is only 167

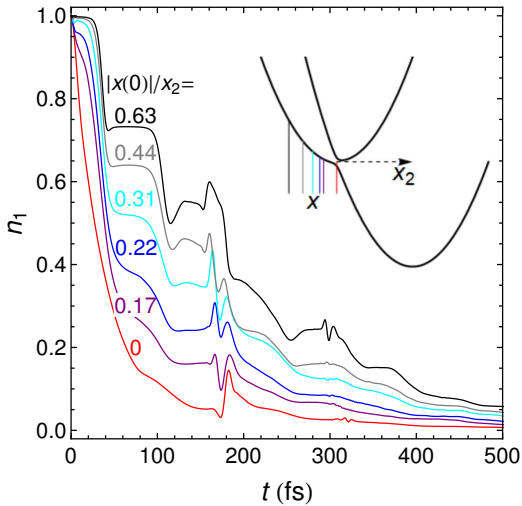


FIG. 3. Time dependence of the occupation $n_1(t)$ of state 1 as a function of different initial displacements $x(0)/x_2$ of the wave packet (values indicated in the Figure). The positions are also indicated in the inset). Other parameters are $E_2 - E_1 = 0$, $\varepsilon_2 = 1$ eV, $\hbar\omega_0 = 30$ meV, $V = 40$ meV, and $T_d = 0.2$ ps.

fs. This clearly indicates a failure of the Frank-Condon argument.

The second thing to notice is that the decay becomes increasingly step-like for increasing displacements, see Fig. 3. This is not expected from the dephasing Green's function in Eq. (2), which gives a simple exponential decrease of the occupation n_1 of site 1. Looking at $x(0)/x_2 = -0.63$, we see that initially the wave packet moves inside the potential well of state 1 almost unperturbed. Then there is a drop in occupation of state 1 when passing the point where the potential wells cross. In fact the decay rate for the drop is roughly 1.2 times larger than that for the optimal intersystem crossing ($x(0)/x_2 = 0$). After part of the wave packet is split off into the lower potential, the majority of the wave packet continues. Another part of the wave packet goes into the lower potential well when passing $x = 0$ on the way back, and so on. Subsequent decreases in n_1 are less abrupt due to the dispersion of the wave packet with time. Decreasing the initial displacement makes the effect of moving in and out of the region with the intersystem coupling less pronounced, but the effect is still present. For very small displacements, the wave packet no longer oscillates in and out of the area where the potential wells couple and the results of Fig. 1 are recovered.

The reason for the absence of such a complex behavior in Eq. (3) is that the initial states are assumed to couple to a continuum of phonon states of the other potential well. Using the “impulse” approximation leads to a simple exponential decay. However, what is lost in taking the approximation taken is the idea of position. The initial wave packet in potential 1 is outside potential 2. Even though position is not a good quantum number, the wave packet cannot simply make a transition to states lower

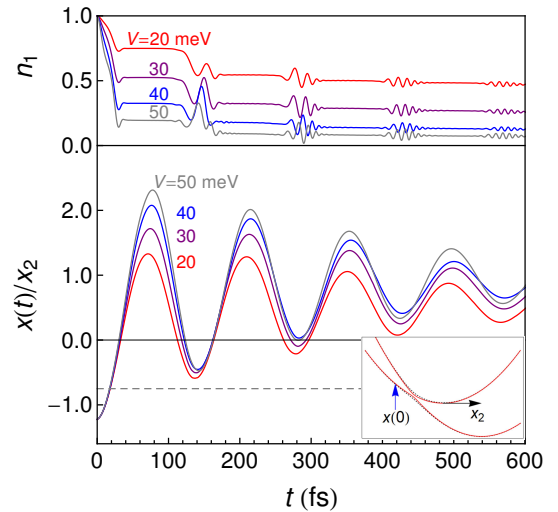


FIG. 4. Coupling constant V dependence for a shifted potential. The values of V are indicated in the Figure. The second potential is shifted by $E_2 - E_1 = -0.3$ eV, causing the classical potential curves to cross for $x/x_2 = -0.75$, see inset. In order to obtain an intersystem crossing, the initial displacement of the wave packet is taken as $x(0)/x_2 = -1.22$, see inset. The other parameters are the same as in Fig. 3. The top part gives the occupation value of state 1; the lower part shows the expectation value of x normalized to the displacement of the minima of the two potential curves x_2 , see inset. The dashed horizontal line gives the position where the potential curves cross.

in energy in potential 2. This would lead to an unacceptable change in the position of the wave packet. This example clearly shows that, even for an optimal intersystem crossing, one cannot treat the intersystem crossing as a process with a constant rate of population transfer when dynamics are involved.

C. Non-optimal crossings

So far, we have considered the “optimal” crossing of the classical potential curves, which gives rise to a fast decay, which is close to exponential in the absence of an initial displacement. Obviously, this is an idealized situation and crossings of potential curves can in principle occur anywhere since, apart from a different coupling to the vibronic mode, the on-site energies of states 1 and 2 can be different. Figure 4 shows an example where the energy of the second potential is lowered $E_2 - E_1 = -0.3$ eV causing the crossing of the potential curves to shift away from the minimum of potential 1, see the inset of Fig. 4. The initial displacement of the wave packet $x(0)/x_2 = -1.22$ is somewhat further away from the minimum of potential 1 than the position $x/x_2 = -0.75$ where the potential curves cross, see inset in Fig. 4. After the initial excitation, the wave packet quickly reaches the region where the potential curves cross and a drop

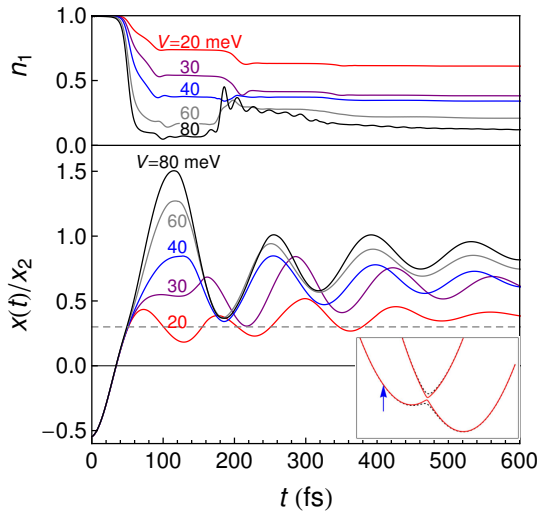


FIG. 5. Coupling constant V dependence for a shifted potential. The values of V are indicated in the Figure. The second potential is shifted by $E_2 - E_1 = 0.6$ eV, causing the classical potential curves to cross for $x/x_2 = 0.3$, see inset. In order to obtain an intersystem crossing, the initial displacement of the wave packet is taken as $x(0)/x_2 = -0.55$, see inset. Other parameters are $\varepsilon_2 = 1$ eV, $\hbar\omega_0 = 30$ meV, and $T_d = 0.2$ ps. The top part gives the occupation n_1 of state 1; the lower part shows the expectation value of x normalized to the displacement of the minima of the two potential curves x_2 . The dashed horizontal line gives the position where the potential curves cross.

in n_1 is observed. As expected, the drop increases with increasing coupling strength V . The wave packet splits and the two parts continue in their respective potential wells. Upon returning to the crossover region, we see a further drop that decreases for increasing V , followed by a temporary increase that increases for increasing V . The second step becomes smaller with increasing V . The increase in n_1 after the second drop can be understood as a short spill back of the wave packet from the second into the first potential well. This spill back increases with the size of the first drop in n_1 . Due to the damping, the amplitude of the oscillation decreases, see the lower half of Fig. 4, and the wave packet no longer reaches the crossover region, although small oscillations in n_1 still occur.

The second potential well can also be shifted higher in energy causing the crossing to occur on the other side of the minimum of the first potential well, see the inset in Fig. 5 where the classical potential curves to cross for $x/x_2 = 0.3$. The expectation value for the displacement of the initial wave packet is $x(0)/x_2 = -0.55$, which allows the wave packet to reach the point where the potentials cross. Initially, the population n_1 of state 1 remains almost constant. This is because the wave packet is outside the second potential well and any transition would lead to an unacceptable change in the position of the wave packet. As expected, the drop in population in-

creases with V , see top part of Fig. 5. The wave packet does not reach far beyond the point where the potentials cross. Only for small V , one can discern that the first step is actually split into two for the wave packet moving in two directions. For larger V , only a single drop is observed. An oscillation period $T_0 = 138$ fs later, the wave packet passes the intersystem crossing position again. Although one might expect n_1 to drop further, this is only observed for small V . For $V \geq 40$ meV, the population of state 1 actually increases. This is a result of the spill back of the population from the second potential well (which also occurs at a time T_0 later, since both potentials have the same period). Further oscillations do not significantly affect the occupation of the states and the wave packet relaxes at the bottom of the two potential wells. The lower part of Fig. 5 shows the displacement $x(t)$. The changes in occupation between the two different states causes a change in the expected position of the wave packet and, for large times, the oscillations damps out around $(1 - n_1(\infty))x_2$, where $n_1(\infty)$ is the final occupation of state 1 and x_2 the displacement

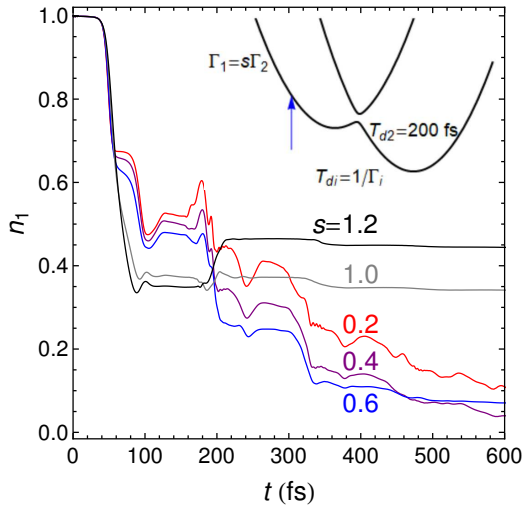


FIG. 6. Dependence of the population transfer n_1 on different dissipation in the two potential wells. The damping of the vibronic motion in the first potential well is $\Gamma_1 = s\Gamma_2$ with the values of s indicated in the Figure. The damping time in the second potential well is $T_{d2} = 1/\Gamma_2 = 0.2$ ps. The coupling constant $V = 40$ meV; the other parameters are the same as in Fig. 5 .

of the second potential well with respect to the first. For small V , the oscillation period is close to $T_0 = 138$ fs. However, for larger V , the first half period (until the first maximum) is unusually extended to $t \cong 115$ fs close to a full oscillations period T_0 of the unperturbed potential well. The effect is much larger than in Fig. 4 due to the larger distortion of the new potential formed by potential well 1 and 2.

D. Unequal dissipation

Figure 6 gives a final example how dynamics and dissipation can drastically change the rates of population transfer. Here, we look at the effect of different dissipation in the potential wells. The decay time is kept constant in the potential well at lower energy, $T_{d2} = 0.2$ ps (or $\Gamma_2 = 1/T_d = 5$ ps $^{-1}$). In the well higher in energy, the damping rate is scaled $\Gamma_1 = s\Gamma_2$ or $T_{d1} = T_{d2}/s$. Note, that there is no particular reason that the damping rates are equal. The dissipation is related to the energy transfer of the local vibronic mode to the larger system. Since the mode has changed significantly between the two wells (for example, this could correspond to a different metal-ligand distance in the case of a breathing mode), the interaction of the local system with the surroundings, and hence the dissipation, can be substantially different. Let us look at the situation comparable to Fig. 5, with the initial wave packet on the opposite side of the point where the potential wells cross, see the inset in Fig. 6. The situation is shown for the situation where there is relatively little damping in the first potential well ($s = 0.2$) to a

stronger damping $s = 1.2$). For small damping ($s = 0.2-0.6$), one can clearly see the wave packet passing the point of intersystem crossing twice in the time span 60-100 fs. For larger, damping ($s = 1.0-1.2$), the wave packet already does not have sufficient kinetic energy to pass the point where the potential wells cross. Having the turning point of the wave packet close to the gap, leads to a larger drop of the population n_1 in potential 1. However, this initial advantage in population transfer for larger s with respect to smaller s disappears with successive oscillations. Whereas for small s , the population transfer continues, for larger s , the damping of the wave packet prevents the point where the potential curves cross from being reached. Additionally, when the damping in potential well 1 exceeds that for 2 ($s = 1.2$), the spill back of population from well 2 into 1 causes an increase of n_1 .

IV. CONCLUSIONS

In summary, intersystem crossings, such as those in metal ions in organometallic compounds, have been studied using a dissipative quantum-mechanical two-potential-well system. Trends have been studied as a function of coupling parameters, the position of the crossing between the potential wells, the strength of the damping, and displacement of the wave packet in the potential well. Many of the results differ from the behavior expected from Fermi's golden rule. The role of dynamics and dissipation in intersystem crossings within the framework of Fermi's golden rule is relatively limited: the dynamics causes the system to move between the potential wells and the dissipation prevents a recurrence of the wave packet in the initial potential well. The population transfer between potential wells is primarily determined by the coupling constants and the Frank-Condon factors. For the intersystem crossing to occur, it is crucial that energy is transported away from the "local" system of electronic and vibronic states. This can be achieved by using a sufficiently large system or by including dissipative effects in the local system. The latter approach, employed here, has the advantage that trends can be more easily studied. The method presented here to damp the motion of the wave packet prevents spurious transitions between the electronic states involved in the intersystem crossing. For "optimal" intersystem crossings, *i.e.* where the potential curve of the second state crosses the minimum of that of the first, and small coupling constants V , Fermi's golden rule gives a good estimate of the dephasing time. The details of the damping are not too crucial: as long as the damping is sufficiently large, it will not affect the population transfer. However, even for optimal intersystem crossings, Fermi's golden rule has its limitations. For larger V , the problem is more appropriately viewed as two new potential wells, see the inset in Fig. 2. The lowest potential well gives a very fast intersystem coupling; the population transfer from state 1 to 2 for the upper potential well decreases with increasing cou-

pling, leading to effectively slower long-time intersystem couplings.

The simple intuitive picture of an exponential decay of the population between the states starts to break down when dynamics become involved. For the optimal intersystem crossing, the wave packet at the bottom of the first potential well can be initially viewed at rest. However, if the wave packet is not created at the position where the potential wells cross, then a different picture emerges where the population changes little when the wave packet is away from the intersystem crossing point. When passing the position where the potential curves cross, the population in the initial well drops quickly. The dephasing times comparable to those of the optimal intersystem crossing in contrast to the strong decrease in population transfer expected from Fermi's golden rule. When moving away from the optimal intersystem crossing, we start to observe a competition between the population decrease from the initial to the final state and back spill from the second into the first potential well. A difference in dissipation in the potential wells can significantly alter the total population transfer in the intersystem crossing. Note that the population transfer is not always complete. Temperature-dependent studies are needed to show a complete depletion of the initial state.

Although the model presented here deals with a simple potential landscape, the results can be helpful in interpreting experiments and calculations on large molecules. Whereas the system can be complex, transitions between potential wells are often dominated by a single mode, for example, a breathing mode or Jahn-Teller distortion for spin crossover phenomena. This is comparable to the model studied here. The other modes have a much smaller effect on the electronic structure. When they are excited, they take away energy from the dominant mode, which is comparable to the dissipation used in this paper. An aspect that is clearly observed in several calculations is the breakdown of Fermi's golden rule. This manifests itself in a population transfer with two different time constants. Many calculations start from the optimal configuration where the initial wave packet is close in energy and position to the crossing of two potential wells. The spin-orbit interaction effectively splits the harmonic wells into an upper and a lower well. Initially, the decay is fast and exponential due to the spin-orbit interaction. This is followed by a slower decay of the part of the initial wave packet that was excited into the upper potential well, see Fig. 2. This decay is dominated by the dissipation mechanism or the vibronic couplings which couple the potential wells. This behavior is observed in the population of the initial state in several calculations^{18,28-31}. For strong coupling, oscillatory behavior in the populations is observed^{18,28} due to the coupling between the upper and lower potentials. Other phenomena presented here should also be present in large calculations for particular systems, such as the appearance of plateaus in the population for displaced wave packets, the spill back

of population density in the original potential well, and changes in population transfer due to different coupling of the electronic states to the surroundings.

ACKNOWLEDGMENTS

This work was supported by the U. S. Department of Energy (DOE), Office of Basic Energy Sciences, Division of Materials Sciences and Engineering under Award No. DE-FG02-03ER46097. Work at Argonne National Laboratory was supported by the U. S. DOE, Office of Science, Office of Basic Energy Sciences, under contract No. DE-AC02-06CH11357.

- ¹A. Hauser, *Spin crossover materials: Properties and application* (Wiley, 2013).
- ²P. Gütllich and H. A. Goodwin, eds., *Spin crossover in Transition-Metal Compounds* (Springer, 2004).
- ³C. Bressler, C. Milne, V.-T. Pham, A. ElNahhas, R. M. van der Veen, W. Gawelda, S. Johnson, P. Beaud, D. Grolimund, M. Kaiser, C. N. Borca, G. Ingold, R. Abela, and M. Chergui, "Femtosecond XANES study of the light-induced spin crossover dynamics in an iron(II) complex," *Science* **323**, 489–492 (2009).
- ⁴W. Gawelda, V.-T. Pham, M. Benfatto, Y. Zaushitsyn, M. Kaiser, D. Grolimund, S. L. Johnson, R. Abela, A. Hauser, C. Bressler, and M. Chergui, "Structural determination of a short-lived excited iron(ii) complex by picosecond x-ray absorption spectroscopy," *Phys. Rev. Lett.* **98**, 057401 (2007).
- ⁵L. A. Fredin, M. Pápai, E. Rozsályi, G. Vankó, K. Wärnmark, V. Sundström, and P. Persson, "Exceptional excited-state lifetime of an iron(ii)n-heterocyclic carbene complex explained," *The Journal of Physical Chemistry Letters* **5**, 2066–2071 (2014).
- ⁶P. Wernet, K. Kunnus, I. Josefsson, I. Rajkovic, W. Quevedo, M. Beye, S. Schreck, S. Grubel, M. Scholz, D. Nordlund, W. Zhang, R. W. Hartsock, W. F. Schlotter, J. J. Turner, B. Kennedy, F. Hennies, F. M. F. de Groot, K. J. Gaffney, S. Techert, M. Odelius, and A. Föhlisch, "Orbital-specific mapping of the ligand exchange dynamics of Fe(CO)₅ in solution," *Nature* **520**, 78 (2015).
- ⁷M. Cammarata, R. Berton, M. Lorenc, H. Cailleau, S. Di Matteo, C. Mauriac, S. F. Matar, H. Lemke, M. Chollet, S. Ravy, C. Lahlou, J.-F. m. c. Létard, and E. Collet, "Sequential activation of molecular breathing and bending during spin-crossover photoswitching revealed by femtosecond optical and x-ray absorption spectroscopy," *Phys. Rev. Lett.* **113**, 227402 (2014).
- ⁸M. van Veenendaal, "Time-dependent nonequilibrium soft x-ray response during a spin crossover," *Phys. Rev. B* **97**, 125108 (2018).
- ⁹T. J. Penfold, E. Gindensperger, C. Daniel, and C. M. Marian, "Spin-vibronic mechanism for intersystem crossing," *Chemical Reviews* **118**, 6975–7025 (2018).
- ¹⁰U. Fano, "Effects of configuration interaction on intensities and phase shifts," *Phys. Rev.* **124**, 1866–1878 (1961).
- ¹¹D. R. Yarkony, "Diabolical conical intersections," *Rev. Mod. Phys.* **68**, 985–1013 (1996).
- ¹²W. Domcke and D. R. Yarkony, "Role of conical intersections in molecular spectroscopy and photoinduced chemical dynamics," *Annual Review of Physical Chemistry* **63**, 325–352 (2012).
- ¹³M. S. Schuurman and A. Stolow, "Dynamics at conical intersections," *Annual Review of Physical Chemistry* **69**, 427–450 (2018).
- ¹⁴S. P. Neville, M. Chergui, A. Stolow, and M. S. Schuurman, "Ultrafast x-ray spectroscopy of conical intersections," *Phys. Rev. Lett.* **120**, 243001 (2018).
- ¹⁵M. C. E. Galbraith, S. Scheit, N. V. Golubev, G. Reitsma, N. Zhavoronkov, V. Despré, F. Lépine, A. I. Kuleff, M. J. J. Vrakking, O. Kornilov, H. Köppel, and J. Mikosch, "Few-

- femtosecond passage of conical intersections in the benzene cation,” *Nature Communications* **8**, 1018 (2017).
- ¹⁶M. Beck, A. Jckle, G. Worth, and H.-D. Meyer, “The multiconfiguration time-dependent hartree (MCTDH) method: a highly efficient algorithm for propagating wavepackets,” *Physics Reports* **324**, 1 – 105 (2000).
- ¹⁷H. Ando, S. Iuchi, and H. Sato, “Theoretical study on ultrafast intersystem crossing of chromium(iii) acetylacetonate,” *Chemical Physics Letters* **535**, 177 – 181 (2012).
- ¹⁸J. Eng, C. Gourlaouen, E. Gindensperger, and C. Daniel, “Spin-vibronic quantum dynamics for ultrafast excited-state processes,” *Accounts of Chemical Research* **48**, 809–817 (2015).
- ¹⁹G. Capano, C. J. Milne, M. Chergui, U. Rothlisberger, I. Tavernelli, and T. J. Penfold, “Probing wavepacket dynamics using ultrafast x-ray spectroscopy,” *Journal of Physics B: Atomic, Molecular and Optical Physics* **48**, 214001 (2015).
- ²⁰S. P. Neville, V. Averbukh, S. Patchkovskii, M. Ruberti, R. Yun, M. Chergui, A. Stolow, and M. S. Schuurman, “Beyond structure: ultrafast x-ray absorption spectroscopy as a probe of non-adiabatic wavepacket dynamics,” *Faraday Discuss.* **194**, 117–145 (2016).
- ²¹M. Pápai, G. Vankó, T. Rozgonyi, and T. J. Penfold, “High-efficiency iron photosensitizer explained with quantum wavepacket dynamics,” *The Journal of Physical Chemistry Letters* **7**, 2009–2014 (2016).
- ²²A. Raab, I. Burghardt, and H. Meyer, “The multiconfiguration time-dependent hartree method generalized to the propagation of density operators,” *The Journal of Chemical Physics* **111**, 8759–8772 (1999).
- ²³U. Lorenz and P. Saalfrank, “Comparing thermal wave function methods for multi-configuration time-dependent hartree simulations,” *The Journal of Chemical Physics* **140**, 044106 (2014).
- ²⁴N. Klinduhov and K. Boukheddaden, “Vibronic theory of ultrafast intersystem crossing dynamics in a single spin-crossover molecule at finite temperature beyond the Born Oppenheimer approximation,” *The Journal of Physical Chemistry Letters* **7**, 722–727 (2016).
- ²⁵M. van Veenendaal, J. Chang, and A. J. Fedro, “Model of ultrafast intersystem crossing in photoexcited transition-metal organic compounds,” *Phys. Rev. Lett.* **104**, 067401 (2010).
- ²⁶M. van Veenendaal, “Ultrafast intersystem crossings in Fe-Co Prussian blue analogues,” *Sci. Rep.* **7**, 6672 (2017).
- ²⁷J. Chang, A. J. Fedro, and M. van Veenendaal, “Ultrafast cascading theory of intersystem crossings in transition-metal complexes,” *Phys. Rev. B* **82**, 075124 (2010).
- ²⁸M. Fumanal, E. Gindensperger, and C. Daniel, “Ultrafast excited-state decays in $[\text{re}(\text{co})_3(\text{n},\text{n})(\text{l})]^{n+}$: Nonadiabatic quantum dynamics,” *Journal of Chemical Theory and Computation* **13**, 1293 (2017).
- ²⁹C. Lévêque, R. Taïeb, and H. Köppel, “Communication: Theoretical prediction of the importance of the 3b2 state in the dynamics of sulfur dioxide,” *The Journal of Chemical Physics* **140**, 091101 (2014).
- ³⁰C. Xie, X. Hu, L. Zhou, D. Xie, and H. Guo, “Ab initio determination of potential energy surfaces for the first two uv absorption bands of so2,” *The Journal of Chemical Physics* **139**, 014305 (2013).
- ³¹J. Krčmář, M. F. Gelin, and W. Domcke, “Simulation of femtosecond two-dimensional electronic spectra of conical intersections,” *The Journal of Chemical Physics* **143**, 074308 (2015).